



Otsubo, M., O'sullivan, C., Sim, W. W., & Ibraim, E. (2015).
Quantitative assessment of the influence of surface roughness on soil
stiffness. *Géotechnique*, 65(8), 694-700.
<https://doi.org/10.1680/geot.14.T.028>

Peer reviewed version

Link to published version (if available):
[10.1680/geot.14.T.028](https://doi.org/10.1680/geot.14.T.028)

[Link to publication record in Explore Bristol Research](#)
PDF-document

University of Bristol - Explore Bristol Research

General rights

This document is made available in accordance with publisher policies. Please cite only the published version using the reference above. Full terms of use are available:
<http://www.bristol.ac.uk/red/research-policy/pure/user-guides/ebr-terms/>

Title: Quantitative assessment of the influence of surface roughness on soil stiffness

Authors: Masahide Otsubo¹, Catherine O'Sullivan², Way Way Sim³, Erdin Ibraim⁴

Affiliation

^{1 - 3} Department of Civil and Environmental Engineering, Skempton Building, Imperial College
London
London SW7 2AZ, United Kingdom

⁴ Department of Civil Engineering, Queens Building, University Walk, Bristol BS8 1TR

Keywords:

Stiffness; Roughness; Bender elements; DEM.

Abstract

The nature of soil stiffness at small strains remains poorly understood. The relationship between soil stiffness (e.g. shear stiffness, G_0) and isotropic confining pressure (p') can be described using a power function with exponent (b), *i.e.* $G_0 = A (p'/p_r)^b$, where A is a constant and p_r is an arbitrary reference pressure. Experimentally determined values of b are usually around 0.5 and these are higher than the value of 0.33 that can be analytically determined using Hertzian theory. Hertzian theory considers contact between two smooth, elastic spheres, however, in reality, inter-particle contacts in soil are complex with particle shape and surface roughness affecting the interaction. Thus Hertzian theory is not directly applicable to predict real soil stiffness. It has, however, provided a useful basis to develop an analytical framework that can consider the influence of particle surface roughness on small-strain soil stiffness. Here, earlier contributions using this framework are extended and improved by paying particular attention to roughness and the tangential contact stiffness. Stiffness values calculated using the newly-derived analytical expressions were compared with the results of bender element tests on samples of borosilicate glass beads (ballotini) whose surface roughness was quantified using an optical interferometer. The analytical expression captures the experimentally observed sensitivity of the small-strain shear modulus to surface roughness.

1. Introduction

In the case of soil under isotropic loading, the relationship between the soil shear modulus at small strains (G_0) and the isotropic confining pressure (p') is generally believed to follow a power function having a coefficient of exponent (b), i.e. $G_0 = A (p'/p_r)^b$, where p_r is an arbitrary reference pressure. McDowell & Bolton (2001) highlighted that the analytical estimate of $b = 0.33$, which can be obtained using Hertzian theory for spheres (Hertz, 1882), is smaller than that usually obtained from experiments, where $b \approx 0.5$. Goddard (1990) showed that particle geometry plays a role: a value of $b = 0.5$ can be analytically expected by considering contacts to be conical instead of spherical. The surface asperities that exist on the rough surface of real sand grains may also affect the b value.

Experimental research that quantitatively relates particle roughness to soil stiffness has rarely been reported due to the difficulty in accurately measuring roughness (Otsubo et al., 2014). Santamarina & Cascante (1998) conducted resonant column tests using rough (rusted) and smooth steel spheres. They found greater wave velocity in the smooth spheres, which is in agreement with the earlier findings of Duffy & Mindlin (1956). Sharifipour & Dano (2006) also found similar results when smooth and rough (corroded by hydrofluoric acid) ballotini were compared. The magnitude of the surface roughness was not quantified in either of those papers.

Yimsiri & Soga (2000) presented a useful approach to quantify the influence of roughness on small strain stiffness based upon contact mechanics for rough surfaces (Greenwood & Trip, 1967; Johnson, 1985) and a micro-mechanics based constitutive model (Chang & Liao, 1994). This model has the disadvantage of giving a physically unfeasible negative Poisson's ratio for apparently reasonable ratios of normal stiffness to tangential stiffness. In their model Yimsiri & Soga assumed that the tangential contact stiffness is not influenced by surface roughness. Recent tribology research has shown that the surface roughness reduces both the normal and tangential contact stiffness (e.g. Gonzalez-Valadez et al., 2010). The current contribution demonstrates that inclusion of this more recent research finding enables a refinement of the expressions proposed by Yimsiri & Soga to establish a more accurate analytical framework.

This contribution firstly revisits the analytical study presented by Yimsiri & Soga (2000) and demonstrates how recent tribological research can be used to modify the expression for tangential contact stiffness in developing their model. In the second part of the paper, the results of wave velocities measured in bender element tests on isotropically loaded ballotini samples, whose roughness was quantified using optical interferometry, are presented to validate the newly derived analytical expressions that relate overall (macro-scale) stiffness to the contact stiffness parameters.

2. Theoretical derivation of shear modulus for smooth elastic contacts

Hertz (1882) developed expressions to describe contact between smooth elastic surfaces. Hertzian theory has been used as a basis to explain the relationship between soil shear modulus and confining pressure (e.g. McDowell & Bolton, 2001). According to Hertzian theory (Johnson, 1985) the normal contact stiffness (K_N) between two identical smooth spheres, is given by:

$$K_N = \frac{2G_p}{1-\nu_p} a \quad (1)$$

$$a = \left[\frac{3r(1-\nu_p)}{8G_p} \right]^{1/3} F_N^{1/3} \quad (2)$$

74 where G_p = particle shear modulus; ν_p = particle Poisson's ratio; a = circular (smooth) contact area
 75 radius; r = radius of the identical contacting spheres; and F_N = normal inter-particle contact force.
 76 Mindlin (1949) described the tangential contact stiffness (K_T) between smooth spheres using Hertzian
 77 theory. This model was extended to general cases which consider various loading histories by Mindlin
 78 & Deresiewicz (1953) who give the following expression of the tangential contact stiffness for virgin
 79 (initial) inter-particle tangential loading, F_T :

$$80 \quad K_T = \frac{4G_p}{2 - \nu_p} a \left(1 - \frac{F_T}{\mu F_N} \right)^{1/3} \quad (3)$$

81 where μ = coefficient of inter-particle friction. Eqs. 1 and 3 lead to the following expression for the
 82 contact stiffness ratio (R_K) for smooth contacts:

$$83 \quad R_K \equiv \frac{K_T}{K_N} = \frac{2(1 - \nu_p)}{2 - \nu_p} \left(1 - \frac{F_T}{\mu F_N} \right)^{1/3} \quad (4)$$

84 Chang & Liao (1994) used a micromechanics based model to relate the shear modulus (G_0) of an
 85 assembly of randomly packed identical spheres to K_N and K_T . Using kinematic and static hypotheses
 86 which assume uniform strain and uniform stress respectively, expressions for upper and lower bound
 87 estimates of the elastic modulus were proposed:

$$88 \quad G_{0,Kinematic} = \frac{2Nr^2 K_N}{3V} \cdot \frac{2 + 3R_K}{5} \quad (5)$$

$$89 \quad G_{0,Static} = \frac{2Nr^2 K_N}{3V} \cdot \left(\frac{5R_K}{3 + 2R_K} \right) \quad (6)$$

90 where N = the total number of particle contacts in the sample of volume V . The ratio N/V can be
 91 obtained from the particle radius (r), the sample void ratio (e) and the mean coordination number (N_C)
 92 as expressed in Yimsiri & Soga (2000) as follows:

$$93 \quad \frac{N}{V} = \frac{3N_C}{8r^3 \pi(1 + e)} \quad (7)$$

94

95 **3. Theoretical derivation of shear modulus for rough elastic contacts**

96 **3.1 Influence of surface roughness on normal contact stiffness**

97 Greenwood et al. (1984) and Johnson (1985) proposed a non-dimensional roughness parameter (α) to
 98 extend Hertzian theory to rough contacts:

$$99 \quad \alpha = \frac{S_q}{\delta_N} \quad (8)$$

100 where S_q = root mean square (RMS) roughness; and δ_N = overlap of contacting spheres as used in
 101 Hertzian theory. The RMS roughness is defined as (Thomas, 1982):

$$102 \quad S_q = \sqrt{\frac{1}{n} \sum_{i=1}^n (Z_i^2)} \quad (9)$$

103 where n is the number of measured data points; and Z_i is the elevation of data point i relative to the
 104 reference surface.

105

106 When two rough surfaces having S_{q1} and S_{q2} are considered, S_q in Eq. 8 can be replaced by a combined
 107 roughness, i.e. $S_q^2 = S_{q1}^2 + S_{q2}^2$ (Greenwood et al., 1984; Johnson, 1985). Yimsiri & Soga (2000) used

108 α to relate the radius of circular contact area between two rough surfaces (a^{Rough}) to the smooth
 109 equivalent (a^{Smooth}) as follows:

$$110 \quad a^{Rough} = \left(\frac{-2.8}{\alpha + 2} + 2.4 \right) a^{Smooth} \quad (10)$$

111 At an extremely large normal load, α approaches zero and $a^{Rough} \rightarrow a^{Smooth}$. Assuming that Hertzian
 112 theory of $r \delta_N = 2a^2$ is still applicable to rough contacts, the overlap of rough spheres can be analysed
 113 as:

$$114 \quad \delta_N^{Rough} = \frac{(2a^{Rough})^2}{r} = \frac{2}{r} \left[\left(\frac{-2.8}{\alpha + 2} + 2.4 \right) a^{Smooth} \right]^2 \quad (11)$$

115 Yimsiri & Soga (2000) derived the normal contact stiffness for rough contacts by differentiating F_N
 116 with respect to δ_N

$$117 \quad K_N^{Rough} = \frac{dF_N}{d\delta_N^{Rough}} \quad (12)$$

118 **3.2 Influence of surface roughness on tangential contact stiffness**

119 The effect of surface roughness on the tangential contact stiffness is complex. Yimsiri & Soga (2000)
 120 referred to an experimental study by O'Connor & Johnson (1963) and assumed that K_T^{Rough} equals
 121 K_T^{Smooth} . However, this assumption results in the Poisson's ratio of the assembly becoming negative
 122 when $K_T^{Rough} > K_N^{Rough}$ (i.e. $R_K^{Rough} > 1$) according to the following equations proposed by Chang &
 123 Liao (1994):

$$124 \quad \nu_{s, Kinematic} = \frac{1 - R_K}{4 + R_K} \quad (13)$$

$$125 \quad \nu_{s, Static} = \frac{1 - R_K}{2 + 3R_K} \quad (14)$$

126 where $\nu_{s, Kinematic}$ and $\nu_{s, Static}$ are the Poisson's ratios obtained using the kinematic and static
 127 assumptions. To overcome this drawback, it is essential to select an appropriate value for K_T^{Rough} .
 128 Knowing R_K and K_N^{Rough} , K_T^{Rough} can be obtained using Eq. 4. The influence of the surface roughness
 129 on R_K has been reported in recent tribology research; Campañá et al. (2011) and Medina et al. (2013)
 130 assumed the same R_K for both smooth and rough contacts. In contrast, a lower R_K for rough contacts
 131 was reported by Gonzalez-Valadez et al. (2010), whose ultrasound tests showed that $R_K^{Rough} <$
 132 R_K^{Smooth} , and R_K^{Rough} increases as the normal contact force increases. Here it is assumed that $R_K^{Rough} =$
 133 R_K^{Smooth} .

134
 135 The coefficient of inter-particle friction, μ , for rough contacts is needed to calculate Eq. 4. Cavarretta
 136 et al. (2010) and Senetakis et al. (2013) obtained the inter-particle friction by shearing one particle
 137 over another. Cavarretta et al. (2010) observed a higher friction for rough contacts than smooth ones.
 138 Note that this type of experiment is non-trivial and very challenging to interpret. In contrast, plastic
 139 theory predicts lower friction coefficient with larger roughness due to yielding of asperities (Chang et
 140 al., 1988; Kogut & Etsion, 2004; Chang & Zhang, 2005).

141
 142 Rough contacts can be modelled as a system of multiple micro-contacts, each being a smooth spherical
 143 surface. Referring to Fig. 1, the inter-particle forces of F_N and F_T can be decomposed into normal ($f_{N,i}$)
 144 and tangential contact forces ($f_{T,i}$) that act on an individual micro-contact i . The magnitude of $f_{T,i} / f_{N,i}$
 145 depends upon the micro-contact orientation. Summing this ratio over all the micro-contacts, gives:

$$\frac{F_T}{\mu F_N} \cong \sum_i \frac{f_{T,i}}{\mu f_{N,i}} \quad (15)$$

Thus, Eq. 4 can be applied to rough contacts using $R_K^{\text{Rough}} = R_K^{\text{Smooth}}$. The resultant expressions for K_T^{Rough} are given in Table 1. Substitution of K_N^{Rough} and K_T^{Rough} into Eqs. 5 and 6 gives the shear modulus of the assembly.

4. Experiments

4.1 Tested materials

The material tested comprised of borosilicate ballotini spheres with diameters between 2.4 mm and 2.7 mm. (shear modulus, $G_p = 25$ GPa, specific gravity = 2.23, particle Poisson's ratio, $\nu_p = 0.2$). Typical microscope images and optical interferometry surface topographies of these particles are shown in Fig. 2. The rough ballotini were made by milling the smooth ballotini as described by Cavarretta et al. (2012). Forty surface roughness measurements were conducted on each material using a Fogale Microsurf 3D (Fogale, 2005). The effects of surface curvature were considered in the roughness measurements, and Fig. 2 summarises the roughness values as-measured and after-flattening using a built-in motif analysis function available in the Fogale software (Fogale, 2005).

4.2 Cubical cell apparatus and sample preparation

A cubical cell apparatus was used, whereby pressures are applied to a cubical sample using flexible air-filled cushions (Ko & Scott, 1967; Sadek & Lings, 2007). The cubical samples (100x100x100 mm³) were prepared using a pluviation device that maintains a constant drop height (Camenen et al., 2013). The measured void ratios were 0.632 and 0.679 and the measured relative densities were 42% ($e_{\min} = 0.557$ and $e_{\max} = 0.698$) and 47% ($e_{\min} = 0.585$ and $e_{\max} = 0.746$), for the smooth and rough ballotini samples respectively. Note that the size of the tested materials exceeds the maximum recommended particle size for which this test is applied (up to 2.00 mm in diameter; JGS 0161, 2009). A vacuum confinement of 50 kPa was applied while the sample was gently moved into the cubical cell apparatus (O'Donovan et al., 2014).

4.3 Bender element testing

Bender element testing was initially developed by Shirley (1978) and Shirley & Hampton (1978). Bender/extender (BE) elements which are able to generate shear waves (S wave) and compression waves (P wave) were used in this research (Lings & Greening, 2001). Details of the installation of the bender elements using the cubical cell apparatus are described by O'Donovan et al. (2014). The bender elements were inserted into the faces of the cubical sample, while it was still subject to vacuum confinement of about 50 kPa; then the vacuum confinement was systematically reduced as the cushion pressure was increased, initially to an isotropic cell pressure of 50 kPa. Bender element tests were carried out at discrete confining pressures (50, 100, 200, 300, 400 and 500 kPa) both during loading and unloading. After increasing the confining pressure to next level, a pause of at least 1 hour was applied to allow for creep of the sample.

At each confining pressure a sinusoidal wave with a frequency of 15 kHz and 270 degrees of phase delay was transmitted. The high frequency chosen should minimise the near field effects in received signal (Arroyo et al., 2003). The importance of choosing a sensible method to identify the wave arrival has been discussed extensively (e.g. Yamashita et al., 2007 & 2009). This research uses a peak to peak method in which the time delay between the peaks of the transmitted and received waves is considered to be the travel time.

4.4 Test results

A typical series of the received S-wave voltages in one direction for smooth and rough samples at various confining pressures is illustrated in Fig. 3. The vertical axis gives transmitted and received voltages normalised by their maximum values; the relevant test confining pressure is indicated on each voltage trace. Arrows show the first and second peaks in received waves. As the confining pressure increases, the first peaks of the received waves appeared earlier, indicating higher velocities. Comparing Fig. 3(a) and (b) the differences in response are due to the combined effects of differences in surface stiffness and differences in sample void ratio.

The relationships between the elastic moduli and the elastic wave velocities are assumed to be applicable here, i.e.:

$$M_0 = \rho V_p^2 \quad (16)$$

$$G_0 = \rho V_s^2 \quad (17)$$

where M_0 and G_0 = constrained and shear moduli, respectively; ρ = sample bulk density; V_p and V_s = compression and shear wave velocities, respectively. The Poisson's ratio of the sample (ν_s) can be calculated by assuming applicability of elastic theory for homogeneous and isotropic materials (Kumar & Madhusudhan, 2010).

$$\nu_s = \frac{M_0 - 2G_0}{2(M_0 - G_0)} \quad (18)$$

The calculated moduli include the effects of soil density. A correction factor based on a void ratio function of the form proposed by Hardin & Richart (1963)

$$F(e) = \frac{(B - e)^2}{1 + e} \quad (19)$$

was applied to G_0 for both smooth and rough assemblies. Regression analyses were used to fit functions through the experimental data of V_s-p' and $e-p'$ to interpolate values of V_s and e at additional values p' . Best surface fitting through the larger interpolated dataset showed that B is approximately 2.9 and that this value is equally valid for both materials. A value of 2.17, derived for rounded sand particles (Hardin, 1965), has previously been used by Kuwano & Jardine (2002) and Yang & Gu (2013) for data on glass ballotini.

The normalised shear modulus $G_0/F(e)$ in XY (X wave propagation direction, Y wave polarisation) and YX (Y wave propagation direction, X wave polarisation) directions are plotted against the isotropic confining pressure in Fig 4. Here, only data for the loading case are presented. As the confining pressure increases the difference between smooth and rough samples gradually reduced, as reported in the analytical study by Yimsiri & Soga (2000). The power coefficients for the smooth ballotini sample ranged from 0.35 to 0.37, while those for rough ballotini sample ranged from 0.53 to 0.66. Note that with the exception of one measurement point at low confinement pressure that could have affected the quality of the contacts, there is very good agreement between the measurements in both directions for both smooth and rough samples.

5. Discussion and comparison between analysis and experiments

In order to use experimental data to validate the newly derived analytical expressions of stiffness, a number of particle-scale parameters were needed. Referring to Eqs. 4-7, the normal and tangential contact forces (F_N and F_T), the void ratio (e) and the mean coordination number (N_C) were obtained from DEM simulations which considered similar cubical samples (O'Donovan, 2013) and similar particle size distributions. These data gave $0.0665 \leq F_T/F_N \leq 0.0687$, $0.697 \geq e \geq 0.677$ and $5.38 \leq N_C \leq 5.63$ as p' increased from 0.1 MPa to 1 MPa. The friction coefficient for the ballotini (μ) was taken as 0.0805 based on Cavarretta et al. (2012). Referring to Fig. 5 there is a good agreement between the experimental data and the analytical predictions using the static assumption. The kinematic assumption overestimates the shear modulus in both cases; however, it does capture the experimental trend, i.e. the rough particles are softer than the smooth particles and the difference in stiffness between the rough and the smooth materials decreases with increasing p' .

The evolution of the Poisson's ratio (ν_s) at different confining pressures is compared in Fig. 6. The analytical values derived from Eqs. 13 and 14 gave lower estimates for ν over the range of examined confining pressures when compared with the experiments. However, the analytical expression for ν does not depend on the surface roughness. The static hypothesis was again in better agreement with the experimental results for smooth particles. It is interesting that the experimental value for rough particles decreased as the confining pressure increased, while the opposite trend was observed for the smooth particles. Similar experimental results were reported by Sharifipour & Dano (2006) where smooth and rough (corroded) ballotini were compared. It is worth mentioning that Suwal & Kuwano (2013) compared the Poisson's ratio obtained in static and dynamic tests and found that the dynamic tests gave a larger value.

6. Conclusions

This contribution has revisited the analytical model proposed by Yimsiri & Soga (2000) that relates elastic stiffness of an assembly of particles to particle scale parameters. Drawing on recent experimental research, the model was extended to include a reduction in the inter-particle tangential stiffness with surface roughness. Incorporation of this feature results in more realistic values of shear modulus and Poisson's ratio, in particular the negative Poisson's ratio values which were obtained when the original model was used with (plausible) contact stiffness ratios exceeding 1 are now avoided. To validate the new model, bender element tests on smooth and artificially roughened ballotini were performed in a cubical cell. The particle surface roughnesses were quantified using an optical interferometer, to enable direct comparison with the modified analytical expression. Additional particle-scale data needed for the analytical expression were obtained from an equivalent DEM simulation. The estimates of small-strain shear modulus obtained using the new analytical model were in good agreement with the experimental data when the static hypothesis was used, while the expression derived using the kinematic hypothesis was qualitatively similar. Both the analytical model and the experimental data show that increasing particle surface roughness reduces the shear modulus at small strains, and the magnitude of this reduction reduces with increasing isotropic confining pressure. The analytical and experimental data both indicate that the power coefficient (b) increases with surface roughness. The analytical expression for Poisson's ratio does not consider surface roughness, and the expression from the static hypothesis gave a better match to the experimental data than that obtained using the kinematic hypothesis.

Acknowledgements:

Partial funding for this research was provided via EPSRC grants EP/G064954/1 and EP/G064180/1. The first author is supported by JASSO (Japan Student Services Organization) and an Imperial College Dixon Scholarship.

References

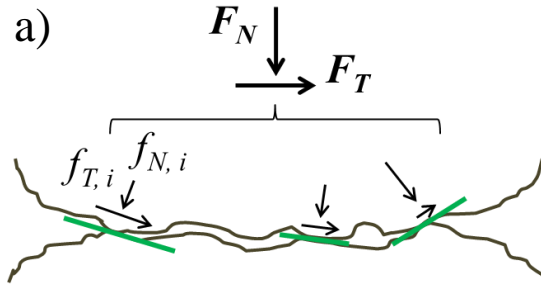
- Arroyo, M., Muir Wood, D., & Greening, P.D. (2003) "Source near-field effects and pulse tests in soil samples", *Géotechnique* 53(3), 337–345.
- Camenen, J.F., Hamlin, S., Cavarretta, I., & Ibraim, E. (2013) "Experimental and numerical assessment of a cubical sample produced by pluviation" *Géotechnique Letters* 3(2), 44–51.
- Campaná, C., Persson, B.N.J., & Müser, M.H. (2011) "Transverse and normal interfacial stiffness of solids with randomly rough surfaces" *Journal of Physics : Condensed Matter* 23, 085001
- Cavarretta, I., Coop, M., & O'Sullivan, C. (2010) "The influence of particle characteristics on the behaviour of coarse grained soils" *Géotechnique* 60(6), 413–423.
- Cavarretta, I., O'Sullivan, C., Ibraim, E., Lings, M., Hamlin, S., & Wood, D.M. (2012) "Characterization of artificial spherical particles for DEM validation studies" *Particuology* 10(2), 209–220.
- Chang, C., & Liao, C. (1994) "Estimates of elastic modulus for media of randomly packed granules" *Applied Mechanics Reviews* 47(1S), S197–S206.
- Chang, L., & Zhang, H. (2005) "On the two points of views of plastically deformed asperity contacts with friction loading" *Proceedings of the Institution of Mechanical Engineers, Part J: Journal of Engineering Tribology* 219, 201–206.
- Chang, W., Etsion, I., & Bogy, D. (1988) "Static friction coefficient model for metallic rough surfaces" *Journal of Tribology* 110(1), 57–63.
- Duffy, J., & Mindlin, R. (1956) "Stress-strain relations and vibrations of a granular medium" *ASME Journal of Applied Mechanics* 24, 585–593.
- Fogale (2005) *Fogale Nanotech User Manual* version 1.5. Nimes, France: Fogale.
- Goddard, J.D. (1990) "Nonlinear elasticity and pressure-dependent wave speeds in granular media" *Proceedings Royal Society of London A: Mathematical and Physical Sciences* 430, 105–131.
- Gonzalez-Valadez, M., Baltazar, A., & Dwyer-Joyce, R.S. (2010) "Study of interfacial stiffness ratio of a rough surface in contact using a spring model" *Wear* 268(3-4), 373–379.
- Greenwood, J., Johnson, K., & Matsubara, E. (1984) "A surface roughness parameter in Hertz contact" *Wear* 100(1-3), 47–57.
- Greenwood, J., & Tripp, J. (1967) "The elastic contact of rough spheres" *Journal of Applied Mechanics* 34(1), 153–159.
- Hardin, B.O. (1965). "Dynamic versus static shear modulus for dry sand". *Materials Research & Standards, ASTM*, 232-235.
- Hardin, B.O., & Richart F.E. (1963). "Elastic wave velocities in granular soils" *Journal of Soil Mechanics & Foundations Division, ASCE* 89, SM1, 33–65.
- Hertz, H.R., 1882. Über die Berührung fester elastischer Körper. *Journal Fur Die Reine Und Angewandte Mathematik* 92, 156–171.
- Johnson, K. (1985) *Contact mechanics*. Cambridge University Press.
- Kogut, L., & Etsion, I. (2004) "A static friction model for elastic-plastic contacting rough surfaces" *Journal of Tribology* 126, 34–40.
- Lings, M., & Greening, P. (2001) "A novel bender/extender element for soil testing" *Géotechnique* 51(8), 713–717.
- Kumar, J., & Madhusudhan, B.N. (2010) "Effect of relative density and confining pressure on Poisson ratio from bender and extender elements tests" *Géotechnique* 60(7), 561–567.
- Kuwano, R., Jardine, R. (2002). "On the applicability of cross-anisotropic elasticity to granular materials at very small strains" *Géotechnique* 52(10), 727–749.
- Ko, H., & Scott, R. (1967). "A new soil testing apparatus" *Géotechnique* 17(1), 40–57.
- McDowell, G., & Bolton, M. (2001) "Micro mechanics of elastic soil" *Soils and Foundations* 41(6), 147–152.

337 Medina, S., Nowell, D., & Dini, D. (2013) "Analytical and numerical models for tangential stiffness of
 338 rough elastic contacts" *Tribology Letters* 49(1), 103–115.
 339 Mindlin, R.D. (1949). "Compliance of elastic bodies in contact" *ASME Journal of Applied Mechanics*
 340 16, 259–268.
 341 Mindlin, R.D., and Deresiewicz, H. (1953). "Elastic spheres in contact under varying oblique forces"
 342 *ASME Journal of Applied Mechanics* 20, 327–344.
 343 O'Connor, J., & Johnson, K. (1963) "The role of surface asperities in transmitting tangential forces
 344 between metals" *Wear* 6(2), 118–139.
 345 O'Donovan, J. (2013) *Micromechanics of Wave Propagation through Granular Material*. PhD Thesis
 346 Imperial College London
 347 O'Donovan, J., Hamlin, S., Marketos, G., O'Sullivan, C., Ibraim, E., Lings, M., Muir Wood, D. (2014).
 348 "Micromechanics of seismic wave propagation in granular materials" *Geomechanics from Micro*
 349 *to Macro Proceedings IS-Cambridge 2014*, Soga, K., Kumar, K., Biscontin, G. and Kuo, M.
 350 (Eds.) 305–310, CRC Press.
 351 Otsubo, M., O'Sullivan, C., & Sim, W.W. (2014) "A methodology for accurate roughness
 352 measurements of soils using optical interferometry" *Geomechanics from Micro to Macro*
 353 *Proceedings IS-Cambridge 2014*, Soga, K., Kumar, K., Biscontin, G. and Kuo, M. (Eds.)
 354 1117–1122, CRC Press
 355 Sadek, T., & Lings, M. (2007) "Wave transmission in Hostun sand: multiaxial experiments" *Rivista*
 356 *Italiana di Geotecnica*, 41(2) 69–84.
 357 Santamarina, C., & Cascante, G. (1998) "Effect of surface roughness on wave propagation parameters"
 358 *Géotechnique* 48(1), 129–136.
 359 Senetakis, K., Todisco, M.C., & Coop, M.R. (2013) "Tangential load–deflection behaviour at the
 360 contacts of soil particles" *Géotechnique Letters* 3(2), 59–66.
 361 Sharifipour, M., & Dano, C. (2006) "Effect of grains roughness on waves velocities in granular
 362 packings" *Proceedings First Euro Mediterranean in Advances on Geomaterials and Structure*
 363 123–128.
 364 Shirley, D. (1978) "An improved shear wave transducer" *Journal of the Acoustical Society of America*
 365 63, 1643–1645.
 366 Shirley, D., & Hampton, L. (1978) "Shear-wave measurements in laboratory sediments" *Journal of the*
 367 *Acoustical Society of America* 63, 607–613.
 368 Suwal, L., & Kuwano, R. (2013) "Statically and Dynamically Measured Poisson's Ratio of Granular
 369 Soils on Triaxial Laboratory Specimens" *ASTM Geotechnical Testing Journal*, 36, 4, 1–13.
 370 The Japanese Geotechnical Society (2009). Test Method for Minimum and Maximum Densities of
 371 Sands, JGS 0161:2009 (JIS A 1224:2009).
 372 Thomas, T.R. (1982) *Rough surfaces*. London: Imperial College Press.
 373 Yamashita, S., & Fujiwara, T. (2007) *International parallel test on the measurement of G_{max} using*
 374 *bender elements organized by TC-29*.
 375 http://geotechnicalsociety.jp/file/e/tc29/BE_Inter_PP_Test_en.pdf
 376 Yamashita, S., Kawaguchi, T., Nakata, Y., Mikami, T., Fujiwara, T., & Shibuya, S. (2009)
 377 "Interpretation of international parallel test on the measurement of G_{max} using bender elements"
 378 *Soils and Foundations* 49(4), 631–650.
 379 Yang, J. and Gu, X.Q. (2013) "Shear stiffness of granular material at small strains: does it depend on
 380 grain size?" *Géotechnique* 63(2), 165–179.
 381 Yimsiri, S., & Soga, K. (2000) "Micromechanics-based stress–strain behaviour of soils at small strains"
 382 *Géotechnique* 50(1), 559–571.
 383

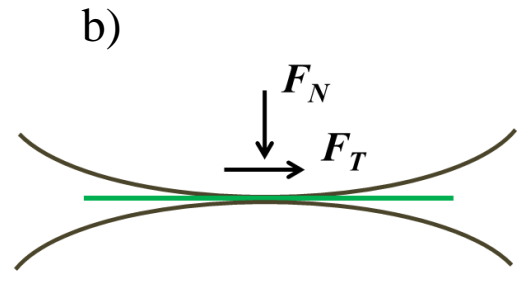
384 **Table 1. Summary of contact model presented by Yimsiri & Soga (2000) and a suggested**
385 **modification. (Tangential contact stiffness is for a virgin tangential load).**

Model	Normal contact stiffness, K_N	Tangential contact stiffness, K_T
Hertz - Mindlin & Deresiewicz (1953)	$K_N^{Smooth} = \frac{2G_p}{1-\nu_p} \left[\frac{3r(1-\nu_p)}{8G_p} \right]^{1/3} F_N^{1/3}$	$K_T^{Smooth} = \frac{2(1-\nu_p)}{2-\nu_p} K_N^{Smooth} \left(1 - \frac{F_T}{\mu F_N} \right)^{1/3}$
Yimsiri & Soga (2000)	$K_N^{Rough} = \frac{dF_N}{d\delta_N^{Rough}}$	
Modified expression		$K_T^{Rough} = \frac{2(1-\nu_p)}{2-\nu_p} K_N^{Rough} \left(1 - \frac{F_T}{\mu F_N} \right)^{1/3}$

386
387

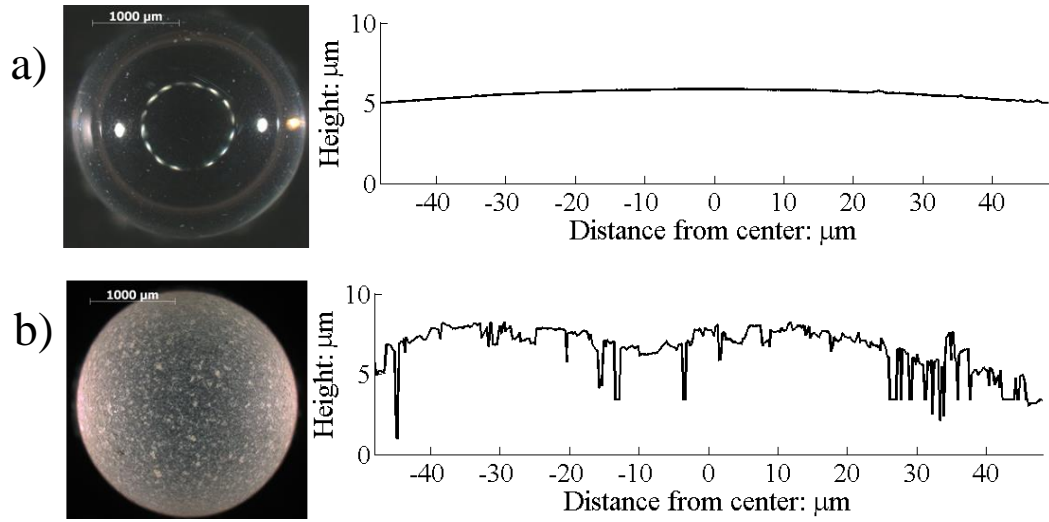


(a) *rough-rough contact*



(b) *smooth-smooth contact*

Figure 1. (a) Inclined contact planes at asperities between rough-rough surfaces and (b) smooth-smooth surfaces.



unit: nm	Smooth ballotini				Rough ballotini			
<i>Sq</i>	Ave	Max	Min	Std	Ave	Max	Min	Std
as-measured	335	402	263	35	1568	2252	1087	264
flattened	36	63	18	12	661	975	538	111

Figure 2. Microscope images and surface topographies of tested materials. (a) smooth ballotini, (b) rough ballotini.

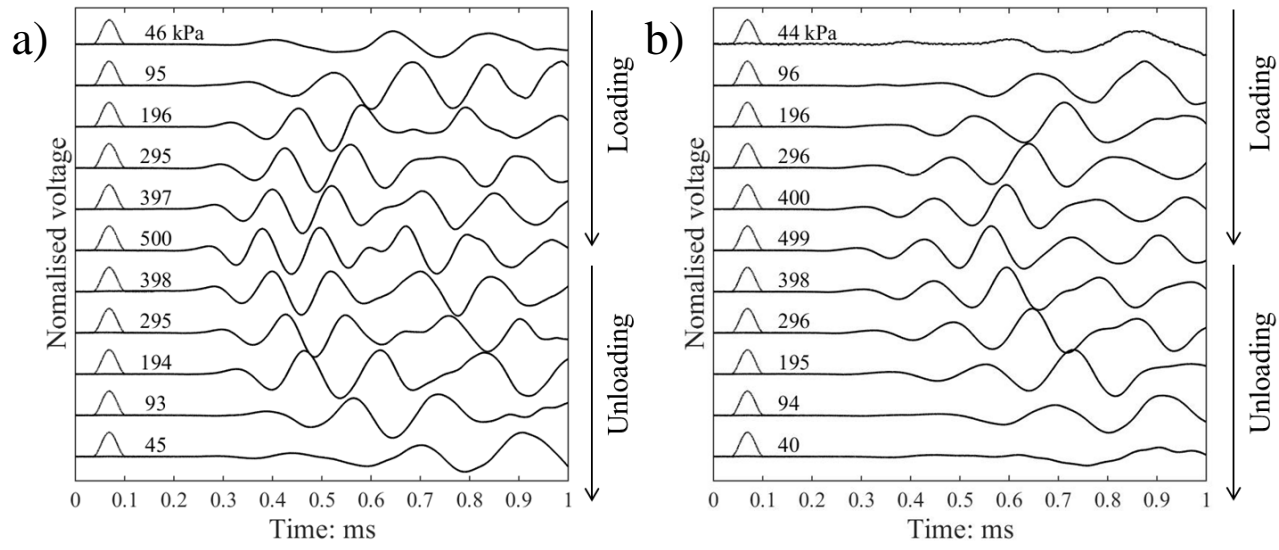


Figure 3. S-wave response in (a) smooth assembly and (b) rough assembly in XY direction at various mean confining pressures. (Arrows indicate the first and second peaks in received waves).

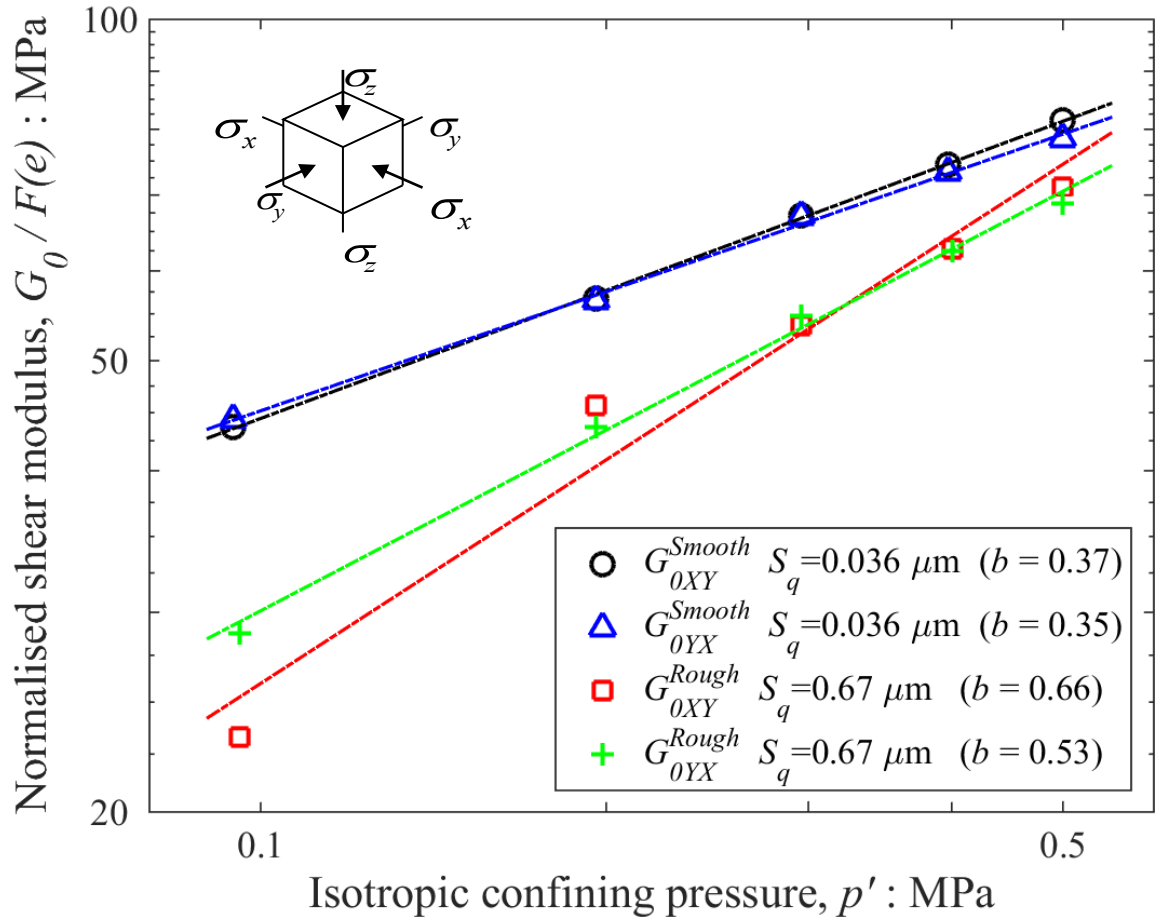
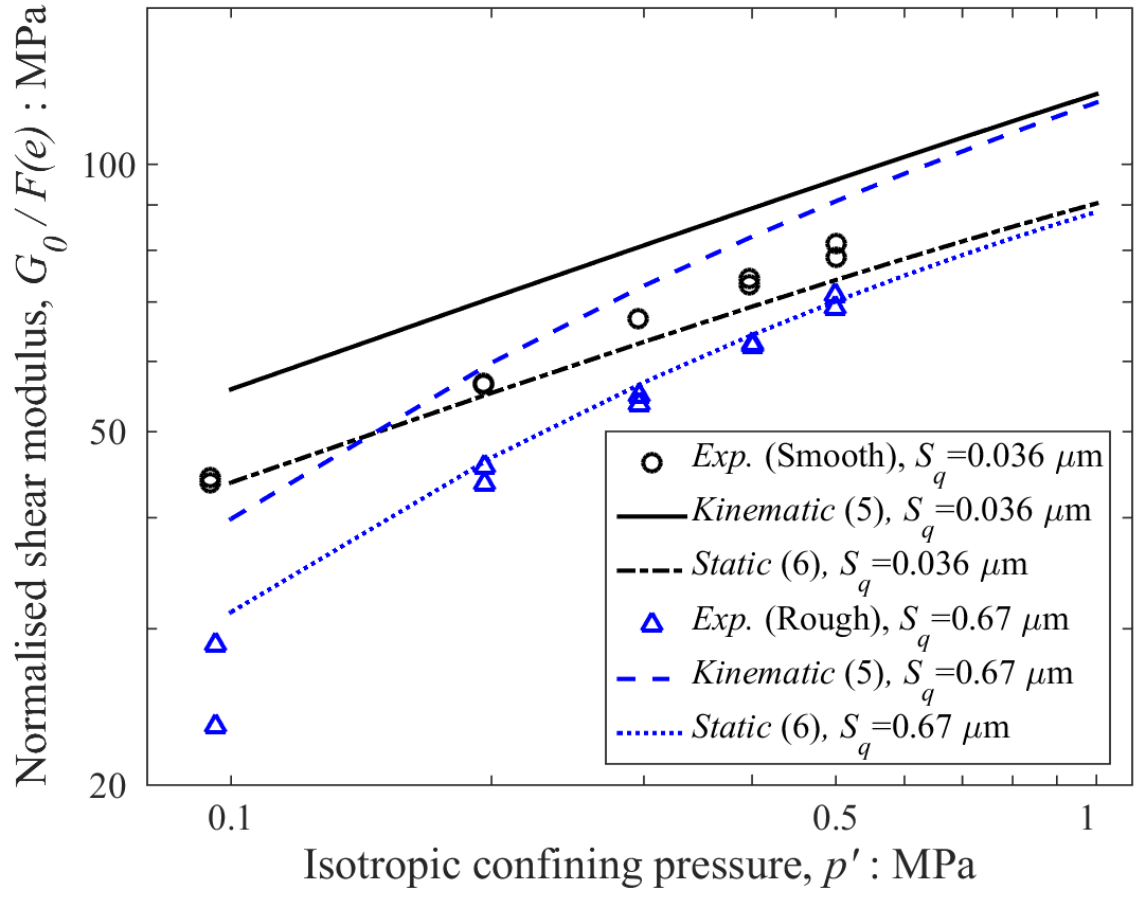


Figure 4. Pressure dependency of shear stiffness in isotropic loading for smooth and rough ballotini samples based on shear wave velocity measurements of waves propagated and polarised in the horizontal plane XY of the cubical sample (in the legend, b is the power coefficient of stiffness – pressure relation, while S_q is the root mean square of roughness).



413
414
415
416
417

Figure 5. Comparison between analytical model and experimental results on relationship between shear modulus and isotropic confining pressure.

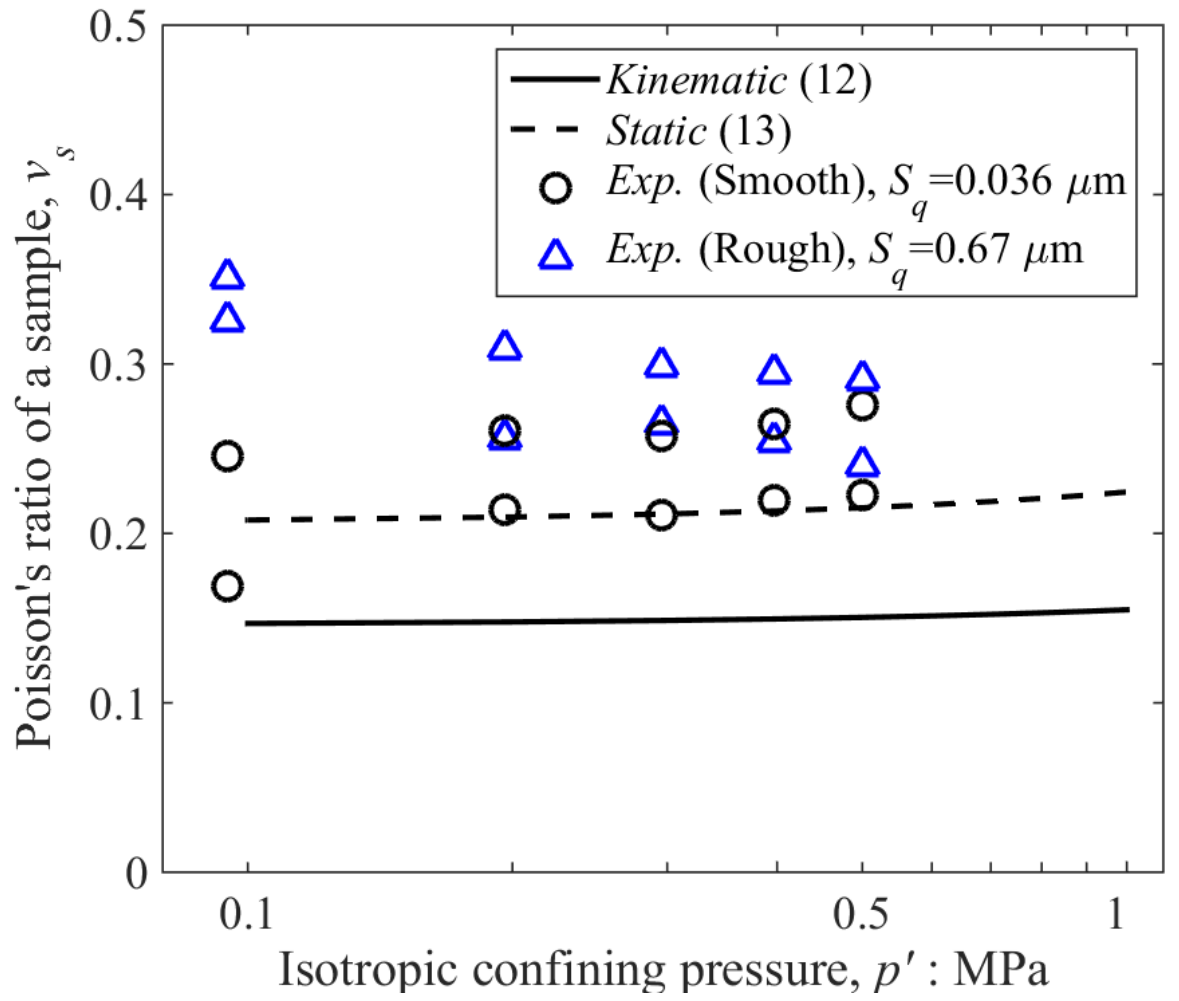


Figure 6. Evolution of Poisson's ratio at various isotropic confining pressures.